Kinetics of Chromate Adsorption and Desorption at Fused Quartz/Water Interfaces Studied by Second Harmonic Generation

Amanda L. Mifflin, Katie A. Gerth, and Franz M. Geiger*

Department of Chemistry, Northwestern University, 2145 Sheridan Road, Evanston, Illinois 60208

Received: June 10, 2003; In Final Form: August 19, 2003

It is now recognized that an understanding of hexavalent chromium pollution in the environment is tied to an understanding of how hexavalent chromium binds to geosorbent surfaces. We have applied the nonlinear optical laser spectroscopy surface second harmonic generation (SHG) to study the adsorption and desorption kinetics of submonolayer amounts of chromate interacting with the fused quartz/water interface at pH 7 and at room temperature. The chromate concentrations are varied between 10^{-6} and 10^{-5} M. The adsorption and desorption behavior of chromate at the fused quartz/water interface can be described by a Langmuir adsorption and a first-order chromate desorption model with an adsorption rate constant of $3(1) \times 10^3$ s^{-1} M^{-1} and a desorption rate constant of $0.9(7) \times 10^{-3}$ s^{-1}. At 300 K and pH 7, the resulting equilibrium constant for chromate binding is in good agreement with equilibrium constants obtained from Langmuir isotherm measurements carried out between pH 4 and 9. Thus, thermodynamic and kinetic measurements carried out in separate studies result in a chromate binding constant of 3.3×10^5 $((+17 \times 10^5)/(-2.1 \times 10^5))$ M^{-1} and a corresponding standard free energy of chromate binding to fused quartz/water interfaces of 32 (+4/−3) kJ/mol. In agreement with the general notion that chromate is highly mobile in most soil environments, a simple transport model predicts that chromate would move between 2 and 9% slower than the noninteracting groundwater phase; that is, it is poorly retained.

I. Introduction

Hexavalent chromium is a carcinogenic and highly toxic heavy metal ion[1−9] whose origin in the environment is mainly due to industrial activities.[5,6,10−13,14] The high mobility of Cr(VI) in many soil environments[15−21] causes great environmental concern.[5] Another concern is the fact that heterogeneous and homogeneous redox chemistry in soils and groundwater can interconvert Cr(VI) and the less toxic oxidation state of chromium in the environment, Cr(III). For this reason, all chromium compounds have been assessed to be potentially carcinogenic.[5,22]

The binding and heterogeneous transformations of chromium species in the environment are governed by surface mechanisms.[23] Chromium binding to minerals is often studied by adsorption isotherm measurements carried out in batch experiments that monitor the aqueous phase chromium concentration in the absence and presence of the solid species. The concentration difference is then taken to be the amount adsorbed.[22,24,25] Time-dependent studies can be easily performed and yield important kinetic information on the binding/redox processes in the reaction vessel. These approaches represent a very powerful method to assess the affinity of chromium ions toward the substrate.

We seek to understand the heterogeneous aspects of chromium binding to geosorbents by studying the interfacial processes of adsorption, reaction, and desorption with interface-specific probes in on-line, that is, in situ, real time laboratory studies and at chromate concentration levels that are environmentally representative (the EPA's maximum contaminant level goal for total chromium in drinking water is 0.1 mg/L or 2 μM,[26] and chromium concentration levels at selected sites in New York, Colorado, and Michigan have been reported to be in the 0.1−1 mM regime).[6] In this work, we describe how chromate binding to fused quartz/water interfaces can be studied in real time. Ultimately, this approach allows for the study of more complicated surface processes such as heterogeneous redox chemistry involving chromate, redox capable substrates, and dissolved or surface-bound organic and inorganic species that are redox capable and commonly found in soil environments. We propose a model for chromate binding to fused quartz/water interfaces and use experimentally determined chromate adsorption and desorption rate constants for predicting chromate retardation factors in soil environments that are rich in silica.

II. Experimental Section

1. Flow Cell and Laser System. The experimental approach has been described previously.[27] Briefly, experiments are carried out at the fused quartz/water interface, chosen as a simple heterogeneous mineral oxide/water system for our studies. While quartz is present in a less pristine form in the natural environment than the fused quartz used here, we chose to begin our studies on chromium binding to mineral oxide/water interfaces by using a simple heterogeneous system that can be expanded in chemical complexity, which is the subject of future work. After careful cleaning with Nochromix solution (Godax Laboratories—*caution: Nochromix is extremely toxic and should only be used after reading and understanding the appropriate safety information*) and rinsing with copious amounts of HPLC grade water (Aldrich and VWR), the flat side of a 1 in. diameter fused quartz hemispherical lens (HL, ISP Optics) is placed over a custom-built Teflon flow cell and held leak-tight using a Viton

* To whom correspondence should be addressed. E-mail: geigerf@chem.northwestern.edu.

10.1021/jp035649f CCC: $25.00
Published on Web 10/18/2003

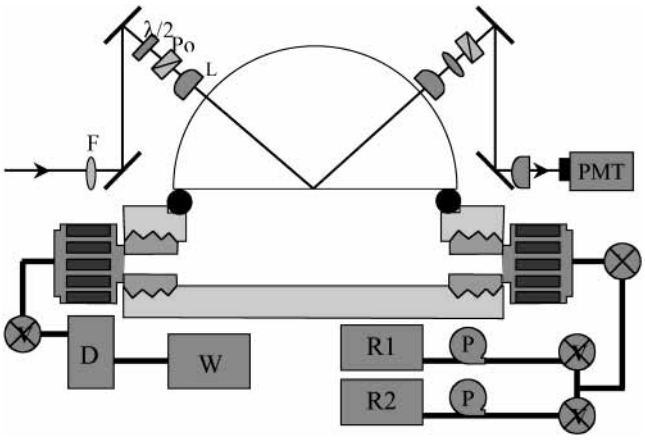

Figure 1. Dual pump flow system with a hemispherical lens attached to the Teflon sample cell (top): F = optical filter; Po = polarizer; $\lambda/2$ = wave plate; L = lens; PMT = photomultiplier with monochromator; V = valve; P = peristaltic pump; R1 and R2 = liquid reservoirs; D = spectrophotometer; W = waste.

O-ring and a clamp (see Figure 1). The sample solutions are stored in liquid reservoirs (R1 and R2) and pumped across the interface using variable-flow peristaltic pumps (P). A dual pump approach allows us to turn the solute flow on and off at a given time using Teflon on−off valves (Swagelok) while maintaining a constant overall flow rate. Simultaneously with the SHG surface measurements, the solute concentration is recorded in real time using a diode array UV−vis spectrometer (D, Ocean Optics, 185−850 nm). Potassium chromate salt (ICN Biomedicals) was used as received for preparing the aqueous chromate solutions, and the solutions were prepared using HPLC grade water (Aldrich) and verified regularly to be at pH 7 using a pH meter (Fisher). Standard sodium hydroxide and hydrogen chloride solutions (Fisher) were used to adjust the pH. The pH was found to remain stable during the course of the experiments. Further, the spectral features observed in the bulk solution spectra, that is, the λ_{max} values and the relative peak intensities of the ligand-to-metal charge-transfer bands, did not change during the experiments, indicating that the relative concentrations of $HCrO_4^-$ and CrO_4^{2-} did not change, consistent with the observed pH stability.

The SHG intensity from surface-bound chromate did not change upon replacing the aqueous phase with a 10^{-3} M NaCl solution, indicating that counterions did not replace the adsorbed chromate in this concentration regime.

The SHG studies are carried out using a kHz 120 fs regeneratively amplified Ti:sapphire system (Hurricane, Spectra Physics) pumping an optical parametric amplifier containing a Type II BBO crystal (OPA-CF, Spectra Physics). In the present study, the frequency-doubled signal output from the OPA at 580 nm is used in order to monitor chromate adsorption via a two-photon resonance of the surface-bound chromate centered at around 290 nm. The 580 nm probe light field is focused onto the fused quartz/water interface to a spot about 50 μm in diameter. Substrate heating[28] is minimized by using femtosecond probe pulses and by probe light field attenuation below the damage threshold via variable neutral density filters.[29] The quadratic power dependencies and spectral bandwidth of the nonlinear signals are verified regularly; departure from the quadratic power dependence and the 3 nm spectral bandwidth for the SHG is observed at laser fluences above 8 μJ. Signal absorption by the aqueous phase is avoided by probing the liquid/solid interface from the fused quartz side at an angle of 60°, which is near the total internal reflection (TIR) angle for the quartz/water interface. Radiation from processes other than SHG is rejected using Schott filters and a monochromator (Monospec, TVC). After directing the SHG signal into a Hamamatsu photomultiplier tube, the signal is preamplified, and the number of second harmonic photons is recorded versus time using a gated photon counter (Stanford Research Systems). In this configuration, the dark counts are around 0.5 photons per second. All experiments are carried out using the p-in/p-out polarization combination. Typical signal intensities are on the order of 0.01 counts per laser shot from the neat fused quartz/water interface (no chromate present) to 0.1 counts per laser shot from the fused quartz/water interface with one monolayer of chromate adsorbed with our experimental setup.

2. Second Harmonic Generation. The adsorption and desorption behavior of chromate is followed in situ and in real time using surface second harmonic generation (SHG).[30−35] The adsorbed chromate was identified via a two-photon resonance of the surface-bound species with the fundamental of the incident light field.[27] The recorded second harmonic intensity I_{SHG} is related to the second-order nonlinear susceptibility of the interface $\chi^{(2)}_{int}$. In the case of resonantly enhanced SHG, $\chi^{(2)}_{int}$ consists of a nonresonant and a resonant contribution, $\chi^{(2)}_{NR}$ and $\chi^{(2)}_{R}$, respectively, whose cross term vanishes when the resonant contribution exceeds the nonresonant contribution to the second-order nonlinear susceptibility, as is the case with our system. $\chi^{(2)}_{NR}$ is nonzero due to the fact that a non-centrosymmetric environment, namely the quartz/water interface, is present. $\chi^{(2)}_{R}$ can be modeled as the product of the number density of molecules adsorbed on a surface and the molecular hyperpolarizability, $\alpha^{(2)}$, averaged over all molecular orientations, according to

$$\sqrt{I_{SHG}} \sim \chi^{(2)}_{int} = \chi^{(2)}_{NR} + \chi^{(2)}_{R} = \chi^{(2)}_{NR} + N_{ads}\langle\alpha^{(2)}\rangle \qquad (1)$$

Since the experiments in this study were carried out using the p-in/p-out polarization combination, the detected SHG intensity arises from the χ_{zzz}, the χ_{zxx}, and the $\chi_{xxz} = \chi_{xzx}$ tensor elements in $\chi^{(2)}$.[35]

Equation 1 shows that SHG can be used to perform kinetic studies of heterogeneous processes by monitoring the time dependence of the square-rooted SHG intensity, which, after subtracting the nonresonant background contribution from the neat fused quartz/water interface (no chromate present), is proportional to the number of adsorbed species at the interface.

III. Results/Discussion

1. Reversibility of Chromate Adsorption at the Fused Quartz/Water Interface. Shown as the bottom trace in Figure 2a is the background-subtracted and square-rooted SHG versus time trace for three consecutive chromate adsorption and desorption experiments. The corresponding absorbance measurement at 275 nm, collected simultaneously with the SHG measurements at 290 nm, is plotted on the top graph.

Until 250 s, only water is flown over the interface at a flow rate of 0.4 mL/s. At 250 s, the water flow is stopped and the chromate flow is initiated simultaneously at a concentration of 7×10^{-5} M in pH 7 water and a flow rate of 0.4 mL/s. The background-subtracted and square-rooted SHG signal intensity is observed to increase and reaches a steady-state level at ~300 s. On the basis of the SHG surface spectrum[27] and the increase of the bulk CrO_4^{2-} absorbance recorded simultaneously with the SHG measurements, the SHG signal increase is attributed to resonance enhancement of the molecular hyperpolarizability

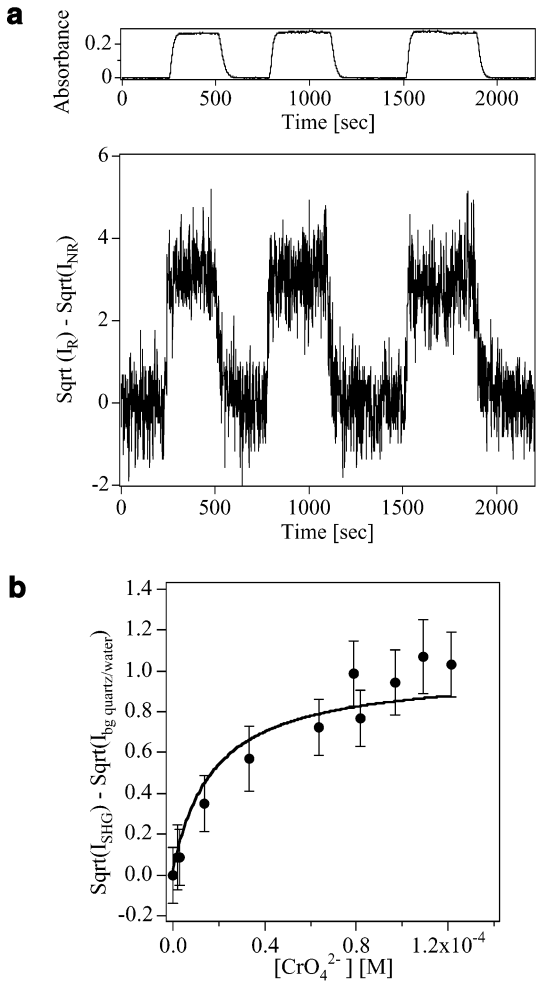

Figure 2. (a) Top: CrO_4^{2-} absorbance vs time trace at 372 nm (left) for three consecutive chromate adsorption and desorption experiments at pH 7. Bottom: Time dependence of the square-rooted and background-subtracted SHG signal from the fused quartz/water interface recorded simultaneously with the absorbance measurements. $\lambda_{SHG} = 290$ nm; $[CrO_4^{2-}] = 7 \times 10^{-5}$ M. As in all other experiments, the polarization combination was p-in/p-out. (b) Adsorption isotherm of CrO_4^{2-} at the quartz/water interface at pH 4 bulk solution. $T = 300$ K. $\lambda_{SHG} = 290$ nm.

of the surface-bound chromate.[27] The resonantly enhanced SHG signal in Figure 2a is termed I_R, and the nonresonant background SHG signal is termed I_{NR}. According to eq 1, the time trace shown in Figure 2a thus depicts the time-dependent chromate surface coverage.

Figure 2a shows that, consistent with eq 1, not only chromate adsorption but also chromate desorption from the quartz/water interface can be followed in real time: Once the chromate flow is turned off, and plain water is flown over the interface at the same flow rate, the SHG signal decreases to the original background level. Turning off the chromate flow without simultaneously turning on the water flow does not cause a change in the SHG signal intensity, indicating that mixing in the cell is complete. Figure 2a also shows that the adsorption of chromate is found to be reversible, which is consistent with the observed high mobility of hexavalent chromium in many soil environments. After one run, the experiment can be started again, resulting in the same maximum SHG intensity upon initiating the chromate flow and resulting in the same background level upon replacing the chromate flow with water. This indicates that chromate binding is indeed fully reversible and that, within the noise level of the data, there is no memory effect from previous chromate adsorption experiments upon carrying out a new adsorption/desorption experiment.

TABLE 1: Free Energies and Chromate Bulk Concentrations Resulting in Monolayer Coverage Formation for Chromate Binding to the Fused Quartz/Water Interface Held at Various pH Levels between 4 and 9

pH	ΔG_{ads} (kJ/mol)	$[CrO_4^{2-}]_{mono}$ (M)
4	37(1)	8.0×10^{-5}
5	35(3)	1.0×10^{-4}
6	33.1(2)	1.5×10^{-4}
7	37.7(1)	5.0×10^{-5}
8	38.4(4)	1.5×10^{-4}
9	36(1)	1.0×10^{-4}

At pH 7, the chromate concentration (7×10^{-5} M) used in these experiments results in approximately monolayer coverage. This was verified by recording adsorption isotherms at a variety of pH values between 4 and 9. For clarity, the isotherm for chromate adsorption to the fused quartz/water interface at room temperature and pH 4 is shown in Figure 2b. The isotherm is very similar to the one obtained for pH 7.[27] The chromate concentration ranged from 5×10^{-6} to 1.2×10^{-4} M. The background-subtracted and square-rooted SHG signal is proportional to the number density of adsorbates (see eq 1). Figure 2b shows that monolayer coverage is reached at around 8×10^{-5} M at pH 4. The adsorption isotherm shown in Figure 2b can be described by a Langmuir model which is based on the equilibrium $CrO_4^{2-}(aq) + site(s) \Leftrightarrow CrO_4^{2-}\cdot site(s)$, where site refers to an adsorption site at the fused quartz/water interface, and aq and s refer to the aqueous and surface-bound localization of chromate, respectively. A Langmuir fit yields a free energy of adsorption of 37(1) kJ/mol at 300 K. The chromate adsorption isotherms recorded between pH 4 and 9 yielded approximately the same free energies of adsorption. The results from the measured adsorption isotherms are listed in Table 1.

2. Chromate Adsorption at the Fused Quartz/Water Interface as a Function of Bulk Flow Rate and Bulk Chromate Concentration. To obtain kinetic information on the processes that govern chromate binding to the fused quartz/water interface, we studied the effect that (a) changes in the total flow rate at constant chromate concentration and (b) changes in the chromate concentration at constant total flow had on the adsorption and desorption traces. The first set of experiments allows us to characterize our experimental flow system with the goal to carry out kinetic studies on heterogeneous redox chemistry involving various environmentally relevant chromium oxidation states. The second set of experiments allows us to test the validity of our proposed kinetic model for chromate interaction with quartz/water interfaces.

Before carrying out these two sets of experiments, we recorded the SHG signal from the plain quartz/water interface as a function of water flow rate (pH 7, no chromate present). In these experiments, the SHG signal intensity is found to be independent of the bulk flow rate (bulk flow rates up to 1 mL/s were applied). This experiment serves as a control experiment for chromate adsorption studies that focus on the effects of changing the chromate flow rate on chromate adsorption and desorption traces such as the ones presented in Figure 2a.

Figure 3a shows chromate adsorption traces recorded at varying total flow rates and a constant chromate concentration. Here, the total flow rate was taken to be the measured chromate flow rate plus the measured water flow rate. The total flow rate was increased from 0.4 to 0.8 mL/s; the measured chromate concentration was 1×10^{-5} M. The adsorption trace for the fastest flow rate is located at the bottom of the graph, and adsorption traces carried out using decreasing flow rates are

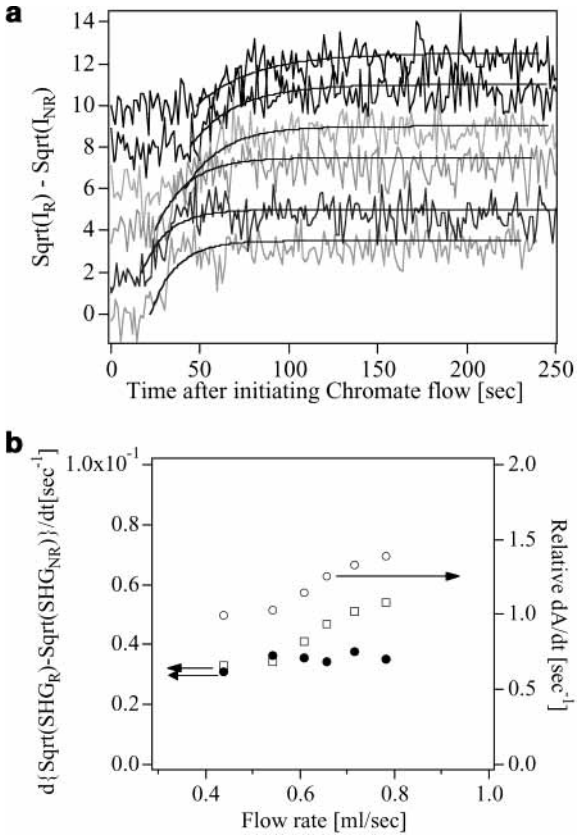

Figure 3. (a) Square-rooted and normalized SHG vs time traces for chromate adsorption recorded at increasing total flow rates and a constant chromate concentration. $\lambda_{SHG} = 290$ nm; $[CrO_4^{2-}] = 1 \times 10^{-5}$ M. Flow rates for the traces, bottom to top: 0.78, 0.71, 0.66, 0.61, 0.54, and 0.43 mL/s. (b) Rate of the SHG signal increase measured as a function of bulk flow rate (empty squares, left). Relative rate of absorbance increase measured as a function of bulk flow rate normalized to the slowest rate of absorbance increase (empty circles, right). Rate of the SHG signal increase divided by the relative and normalized rate of bulk absorbance increase (filled circles, left).

offset for clarity by 2 units on the *y*-axis. It can be seen in Figure 3a that faster flow rates lead to faster SHG signal increases. Further, the time at which the SHG signal increase begins is shortened with increasing flow rates, which is consistent with a faster throughput of the probe species in our flow system as the bulk flow rate is increased.

3. Kinetic Model for Chromate Interaction with the Fused Quartz/Water Interface. The data presented in Figure 3a can be fit to a variety of adsorption models, several of which are summarized by Jung and Campbell in the context of alkanethiol adsorption from the liquid phase onto gold[36,37] or by Georgiadis et al. in the context of nucleic acid monolayer formation on gold−thiol systems.[38] On the basis of the observed reversibility of chromate adsorption and the fact that the recorded chromate adsorption isotherms appear Langmuirian,[27] we chose the Langmuir adsorption model coupled to first-order desorption. In addition to this model, we also fit a diffusion-limited and a diffusion-controlled adsorption model[36−38] to the data. Within the limit of noise in the data, the Langmuir adsorption model coupled to first-order desorption, which includes explicit adsorption and desorption terms, yielded the best fits.

While our chromate adsorption and desorption traces (such as the ones shown in Figure 2a) indicate full reversibility and while the recorded isotherms appear Langmuirian (both implicit assumptions in the Langmuir adsorption/desorption model), there is one significant drawback to this model for the limit of small bulk concentrations: The first-order Langmuir model does not take into account that the bulk phase could be depleted due to adsorption of the solute at the interface. To check whether bulk phase depletion is significant during the adsorption process, we compared the number of chromate ions in the sample cell with the estimated maximum number of surface-bound chromate ions: At any given time, the number of chromate ions in the cell volume (3 cm^3) is around 2×10^{16}. If one assumes 10^{14} to 10^{15} adsorption sites per cm^2 at the interface and a 5 $Å^2$ surface area taken up by the chromate tetrahedron, the maximum number of ions bound to the 1 cm^2 surface at monolayer coverage can be estimated to be around 10^{14}. In our experiments, bulk depletion would thus be below 1% at the bulk concentrations used in the adsorption experiments (10^{-5} M), but some concentration gradient is expected to form. This is consistent with results obtained from calculating the characteristic diffusion time τ_{diff} according to[37,39]

$$\tau_{diff} = \frac{\left(\frac{\Gamma_{1/2}}{C_{bulk}}\right)^2}{D} \qquad (2)$$

where $\Gamma_{1/2}$ is the absolute 50% saturation surface coverage during an individual adsorption experiment, C_{bulk} is the bulk chromate concentration, and D is the chromate diffusion coefficient in the solvent, that is, water, at room temperature. Our experiments only yield surface coverages relative to monolayer formation. If we assume that one monolayer of adsorbed chromate corresponds to about 10^{14} adsorbed chromate ions per cm^2, then characteristic diffusion times ranging from 10 to 40 s are obtained (a diffusion coefficient for 0.01 M K_2CrO_4 in water of 1.4×10^{-5} cm^2 s^{-1} measured by Iadicicco et al.[40] was used in this calculation). This is similar to the observed half-life of the adsorption process (on the order of tens of seconds), consistent with the notion that some concentration gradient will form.[37] It should be noted, however, that this calculation yields an upper limit to the characteristic diffusion time, and absolute surface coverages below 10^{14} cm^{-2} would result in smaller characteristic diffusion times and thus a smaller concentration gradient. The argument that the concentration gradient in our flow system is small is consistent with our observation that stopping the flows after chromate adsorption does not result in changes in the SHG signal intensity, indicating that mixing is complete. These considerations indicate that bulk depletion is likely not to pose a problem. The adsorption portion of the chromate binding experiments was thus analyzed using the Langmuir model with first-order desorption.[36−38,41,42] This model can be written as $CrO_4^{2-}(aq) + site(s) \Leftrightarrow CrO_4^{2-}\cdot site(s)$, where site refers to an adsorption site at the fused quartz/water interface, and aq and s refer to the aqueous and surface-bound localization of chromate, respectively. In this reversible system, the chromate adsorption rate is first order in aqueous chromate concentration and in the surface number density of adsorption sites. The chromate desorption rate is first order in the surface number density of chromate bound to an adsorption site. The time-dependent surface coverage obtained from the Langmuir adsorption/desorption model is the sum of the adsorption and desorption rates:

$$\frac{d\theta}{dt} = k_a C_{bulk}(1 - \theta) - k_d\theta \qquad (3)$$

where θ is the relative chromate surface coverage, $(1 - \theta)$ is the relative surface coverage of unoccupied adsorption sites, k_a is the adsorption rate constant, and k_d is the desorption rate

constant. If the resonant SHG signal intensities exceed the nonresonant signal intensities, as is the case in this study, and if the difference between the square-rooted resonant and nonresonant SHG signal intensities is the chromate surface coverage, then the following time-dependent expression is the solution to eq 3 and was fit to the chromate adsorption traces shown in Figure 3a:

$$\sqrt{I_R} - \sqrt{I_{NR}} = a + b(1 - \exp^{-r_{obs}t}) \quad (4)$$

where the left-hand-side of the equation represents the amount of chromate adsorbed, a is an offset parameter that is included explicitly in order to account for the fact that the data shown in Figure 3a are offset on the y-axis for clarity by the quantity a, b is the final square-rooted SHG signal intensity level yielding the final coverage θ_f (i.e. $b = \{C/(C + (k_d/k_a))\}$), and r_{obs} is the observed rate for chromate binding, given by

$$r_{obs} = k_a C_{bulk} + k_d \quad \text{(refs 38 and 42)} \quad (5)$$

At zero bulk concentration, adsorption cannot occur. For this case, the rate of change in the surface coverage of previously adsorbed chromate becomes the desorption rate, which is given by the desorption rate constant. Figure 3b shows the dependence of the observed rates for the SHG signal increase (obtained from fitting eq 4 to the data shown in Figure 3a) on the flow rate. The open squares are the observed rates for the SHG signal increase. The filled circles are the observed rates for the SHG signal increase divided by the relative rate at which the bulk chromate concentration increases normalized to the slowest flow rate, represented by the open circles. This correction was carried out in order to account for the fact that plug flow conditions are not met in our flow cell. The rates that are corrected for the parabolic concentration profile in our flow system are the adsorption rates used for further analysis. Figure 3b shows that the corrected adsorption rates appear to be independent of the flow rate. If laminar flow conditions were prevalent in our cell (the Reynolds number is $Re = 0.1$), a concentration boundary layer would develop whose thickness δ is a function of the mean stream velocity u_0.[37,43] This thickness is given by

$$\delta = Sc^{-1/3}\sqrt{\frac{\nu x}{u_0}} \quad (6)$$

where Sc is the Schmidt number ($Sc = \nu/D$, with D being again the diffusion coefficient for the species under investigation and ν being the kinematic viscosity of water at room temperature (0.009 cm^2 s^{-1}))[44] and x is the distance from the flow cell entrance to the focus spot of the laser (0.5 cm). With a diffusion coefficient for chromate in aqueous solution of 10^{-5} cm^2 s^{-1},[40] and the range in flow velocities in these experiments, δ ranges from 70 to 80 μm. For the data in Figure 3b, the mean stream velocity increases from 0.70 to 0.90 cm s^{-1} and the boundary layer becomes slightly thinner.

Were the experiment limited by mass transfer, the adsorption rates should depend on the flow rate. This is due to the fact that the adsorption rates are composed of three processes that can be described by the mass transfer coefficient k_c, the adsorption rate constant k_a, and the desorption rate constant k_d. One can set up two boundary conditions in order to find the relationship between mass transfer coefficient, the rate constants, the bulk concentration, and the surface coverage.[45] One boundary condition is that the molar flux to the boundary layer equals the convective transport across the boundary layer (approximated by a linear concentration profile, i.e., $W_B = k_c(C_0 - C_M\theta)$),[45] where C_0 is the bulk chromate concentration and C_M is the concentration in moles per liter corresponding to monolayer coverage (introduced to maintain units). The other boundary condition is that the molar flux to the surface W_S equals the rate of adsorption and desorption; that is, $W_S = d\theta/dt\ C_M V/A$. Here the expression for the time-dependent surface coverage from eq 3 is multiplied by the concentration in moles per liter corresponding to monolayer coverage and a sample volume-to-surface area ratio in order to describe the molar flux from the aqueous phase to the surface. One thus arrives at the following expression:

$$W_B = k_c(C_0 - C_M\theta) = [k_a C_0(1 - \theta) - k_d\theta]C_M V/A \quad (7)$$

Solving for θ, one finds the dependence of the chromate surface coverage on the mass transfer coefficient, the bulk chromate concentration, and the adsorption and desorption rate constants:

$$\theta = C_0\frac{\left(\frac{Ak_c}{C_M V} - k_a\right)}{\frac{Ak_c}{V} - k_a C_0 - k_d} \quad (8)$$

Using the Frössling correlation for large, centimeter diameter single catalyst pellets,[45,46] one can express the mass transfer coefficient as a function of mean stream velocity for systems in which the hydrodynamic boundary layer thickness is much smaller than the diameter of the pellet such that curvature effects can be neglected:

$$k_c = \frac{D}{d_p}(2 + 0.6\sqrt{Re}\sqrt[3]{Sc}) \quad (9)$$

where D is again the diffusion coefficient of the adsorbing species, d_p is the diameter of the pellet, Sc is again the Schmidt number, and Re is the Reynolds number, given by $Re = u_0/\nu d_p$. The mass transfer coefficient thus depends on the mean stream velocity. The fact that the measured chromate adsorption rates are independent of the flow velocity indicates that the system is kinetically controlled; that is, chromate adsorption to the quartz/water interface is not mass transfer limited in our flow cell.

4. Chromate Adsorption at the Fused Quartz/Water Interface as a Function of Chromate Concentration. After establishing that our flow cell is kinetically controlled, we tested our kinetic model for chromate binding to quartz/water interfaces. The process under investigation can be written as CrO_4^{2-}(aq) + site(s) $\Leftrightarrow$ CrO_4^{2-}site(s), where site refers to an adsorption site at the fused quartz/water interface, and aq and s refer to the aqueous and surface-bound localization of chromate, respectively. In this equilibrium system, the chromate adsorption rate is first order in aqueous chromate concentration and in the surface number density of adsorption sites. The chromate desorption rate is first order in the surface number density of chromate bound to an adsorption site. The ratio of the adsorption and the desorption rate constants yields the equilibrium constant for chromate adsorption, which is given by $K_{ads} = k_a/k_d$.

The model predicts that the observed adsorption rate can be expressed as $r_{obs} = k_a C + k_d$ (eq 5). A plot of the observed binding rates versus bulk chromate concentration at constant flow rate should thus give a straight line whose slope yields the adsorption rate constant, k_a, and whose intercept yields the desorption rate constant, k_d. We thus carried out chromate adsorption studies in which the chromate concentration was

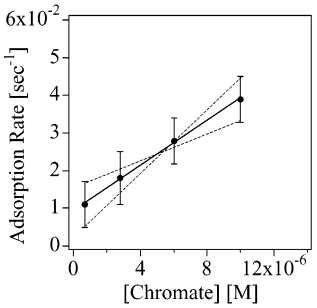

Figure 4. Chromate adsorption rates measured as a function of bulk chromate concentration. The solid line is a fit to eq 5. The dashed lines indicate the upper and lower bounds to the fit.

changed while maintaining the flow rate constant at 0.8 mL/s. The experiments were carried out using chromate concentrations that result in submonolayer coverages to avoid surface saturation, for which the desorption rates would become independent of the bulk chromate concentration. Similar adsorption traces to the ones presented in Figure 3a were found, and eq 4 was fit to the adsorption traces. The resulting adsorption rates are plotted versus the bulk chromate concentration in Figure 4. It can be seen that the chromate adsorption rate increases linearly with increasing chromate concentration in the bulk. An increase in the observed rates with increasing chromate concentration is consistent with eq 8.

Fitting eq 5 to the data in Figure 4 yields a k_a of $3(1) \times 10^3$ s^{-1} M^{-1} and a k_d of $0.009(7)$ s^{-1}. At a chromate concentration of 1×10^{-5} M, the concentration for the chromate adsorption versus flow rate experiments, the adsorption rate constant would result in an adsorption rate of $3(1) \times 10^{-2}$ s^{-1}, which compares well with the adsorption rates obtained from the data shown in Figure 3b. At a chromate concentration of 10^{-5} M, the adsorption and desorption rate constants result in an equilibrium constant for chromate adsorption K_{ads} at 300 K of 3.3×10^5 $((+17 \times 10^5)/(-2.1 \times 10^5))$ M^{-1}. Using a standard state for $\Delta G°$ of 1 mol dm^{-3},[47] the equilibrium constant for chromate adsorption then corresponds to a standard free energy of chromate adsorption of 32 (+4/−3) kJ/mol, which, within experimental error, is comparable to the free energies of adsorption determined from the adsorption isotherms (see Table 1). The standard free energies of adsorption determined in this work are higher than the ones reported for chromate adsorption into aluminum oxide, goethite, and titanium dioxide by Deng and Stone,[24] and we attribute this discrepancy to the difference in the systems studied.

5. Chromate Desorption from the Fused Quartz/Water Interface. The desorption parts of the chromate adsorption and desorption experiments shown in Figure 2 were analyzed using a first-order desorption model. Figure 5a shows the desorption traces recorded using the same flow rates and the same chromate concentration as in the adsorption experiments. The rates of the SHG signal decay are found to increase with increasing flow rate, and the onset time to chromate desorption becomes shorter. A single-exponential function, consistent with a first-order desorption rate law, of the form

$$\sqrt{I_R} - \sqrt{I_{NR}} = a + b \exp^{(-ct)} \quad \text{(refs 36, 37, and 42)} \qquad (10)$$

is fit to the data shown in Figure 5a. Here, a is a constant accounting for the offset in the data, b is the final square-rooted SHG signal intensity level, and c is the rate of signal increase, that is, the rate of chromate desorption. The observed rates of chromate desorption are plotted as a function of the bulk flow

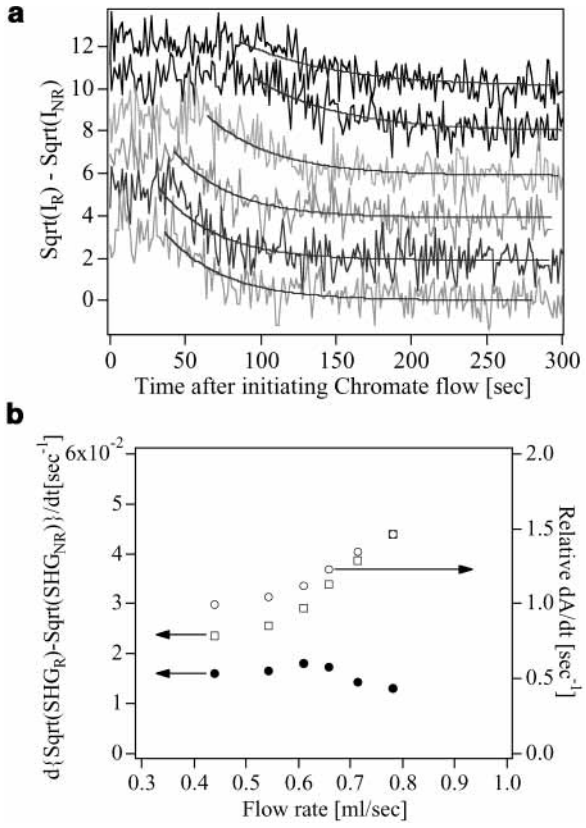

Figure 5. (a) Square-rooted and normalized SHG vs time traces for chromate desorption recorded at increasing total flow rates and a constant chromate concentration. $\lambda_{SHG} = 290$ nm; $[CrO_4^{2-}] = 1 \times 10^{-5}$ M. Flow rates for the traces, bottom to top: 0.78, 0.71, 0.66, 0.61, 0.54, and 0.43 mL/s. (b) Rate of SHG signal decrease measured as a function of bulk flow rate (empty squares, left). Relative rate of absorbance decrease measured as a function of bulk flow rate normalized to the slowest rate of absorbance decrease (empty circles, right). Rate of the SHG signal decrease divided by the relative and normalized rate of bulk absorbance decrease (filled circles, left).

rate in Figure 5b (open squares). After correction for the rate of the bulk chromate signal increase (open circles), it can be seen that the corrected chromate desorption rates (filled circles) are independent of the bulk flow rate, similar to the corrected rates of chromate adsorption. This indicates that for the desorption experiments, like for the adsorption experiments, mass transfer is negligible; that is, $k_c < k_d$. The average desorption rate has a value of $0.016(2)$ s^{-1}, which, within experimental error, is close to the desorption rate constant obtained from the linear fit of eq 5 to the data plotted in Figure 4.

6. Environmental Significance. Our results show that it is possible to study the kinetics of chromate binding to the quartz/water interface using surface SHG in on-line, that is, in situ, real time laboratory studies. The studies can be performed using environmentally representative chromate concentrations. Using water flow rates that are typical of subsurface environments, the experiments can be carried out under flow velocity conditions at which chromate binding to the quartz/water interface is kinetically controlled. Adsorption and desorption rate constants can be determined with surface specificity. The adsorption and desorption rate constants determined here will be used in future kinetic studies that focus on chromate binding to mineral oxide/water interfaces in the absence and presence of coadsorbates as well as chromate reduction by either redox-capable substrates or organic species in the aqueous phase.

A simple but widely used[48] model that predicts pollutant transport in aqueous solution through porous soils and that is

based on experimentally determined binding constants can be used to calculate the migration distance of chromate in groundwater relative to a nonretarded species such as groundwater.[23] This distance is given by

$$x = \frac{\omega t}{1 + \frac{\rho}{n} K_d} \tag{11}$$

where x is the distance traveled, ω is the average groundwater velocity, t is the time, ρ is the bulk density of the geomedia or the sorbent, n is its porosity, and K_d is a binding parameter that describes the interaction of the sorbent with chromate. Using typical values for silicate rock materials, ρ/n has values around 4 and 10 g/cm^3. For the general reaction $A + C_i = A_i$, K_d is defined as the ratio of the mass of adsorbate adsorbed per mass of solid to the mass of the adsorbate in solution at equilibrium:

$$K_d = \frac{\text{mass of adsorbate sorbed}}{\text{mass of adsorbate in solution}} = \frac{A_i}{C_i} \tag{12}$$

where A is the number of unoccupied surface adsorption sites, C_i is the total dissolved adsorbate remaining in solution at equilibrium, and A_i is the amount of adsorbate on the solid at equilibrium.

The advantage of the K_d model is that pollutant transport modeling is straightforward, as nonlinearities between surface coverage and bulk concentration of a pollutant are not included. The most significant drawback of the K_d model is that it does not explicitly take into account all possible processes that may be taking place, resulting in an approximation to the actual K_d value for a system that may or may not be accurate.[48] Further, since K_d values are calculated for specific environmental conditions, a K_d value calculated for one site may not be applicable to another site. The effect of colloids on pollutant transport is not included in the model, either. For these reasons, calculated K_d values tend to be used as upper or lower limit estimations for contaminant migration in groundwater.[48] For the purpose of assessing the financial and human resources needed to remediate a contaminated site, an upper limit of the K_d would likely be used.

Using the linear portion of our Langmuir isotherm plot, we are able to calculate a K_d value for the aqueous chromate-fused quartz system. To compare our calculated values with literature values, we converted the units of the upper limits of our surface coverage estimate to grams of chromate per gram of substrate, and our chromate concentration to g·mL^{-1}, resulting in K_d units of milliliters per gram. The absolute surface coverage, θ_{abs}, is calculated by multiplying the relative surface coverage, θ, which is unitless and normalized to 1, by 10^{14} ions·cm^{-2}, that is, the upper limit to the number of chromate ions on the quartz surface. Using the molar mass of CrO_4^{2-}, the absolute surface coverage corresponds to 1.93×10^{-8} g·cm^{-2}. A fused quartz cube of 1 cm^3 volume, six 1 cm^2 surfaces, and a density of 2.648 g·cm^{-3} would then have a chromate surface coverage of 4.4×10^{-8} $g_{chromate}/g_{quartz}$. After converting the chromate concentration units from moles per liter into grams per mole (using the molar mass of the K_2CrO_4 salt used for preparing the solutions), we are able to obtain a K_d value, in units of milliliters per gram, from the slope of the linear portion of the Langmuir isotherm plot. At pH 4, a K_d value of 0.004 mL/g is obtained, at pH 7, the K_d value is 0.006, and at pH 9, the K_d value is 0.009. These values are below 1 mL/g, which is in good agreement with the K_d values obtained by Rai et al.,[49] who reported K_d values in silica-rich soils between 0 and 1 in a comparable pH regime. Using ρ/n values around 4 and 10 g·cm^{-3}, retardation factors between 1.02 and 1.09 are obtained, indicating that, in silica-rich environments between pH 4 and 9, chromate would move between 2 and 9% slower than the noninteracting groundwater phase; that is, it is poorly retained and highly mobile. This is in good agreement with laboratory studies and field measurements.[49]

Our experimental technique for obtaining K_d values provides an advantage over traditional methods in that SHG yields surface-specific, rather than bulk-specific, data for the adsorption and desorption processes of a contaminant with soil surfaces. Fused quartz, which interacts poorly with chromate, serves as a testing ground for applying nonlinear optical probes to environmental problems. Clearly, kinetic and thermodynamic data derived from more realistic interfaces other than the pristine fused quartz/water interface used in this work will provide more reliable estimates for predicting the migration potential of chromate in the environment. This is the subject of future work which focuses on obtaining kinetic and thermodynamic parameters for more complicated interfaces that are decorated with inorganic and/or organic ionic or molecular species coadsorbed with the surface-bound chromate.

IV. Conclusions

The adsorption and desorption kinetics of chromate to the fused quartz/water interface held at pH 7 and at room temperature were studied using nonlinear optical laser spectroscopy surface second harmonic generation (SHG). The chromate concentration was varied between 10^{-6} and 10^{-5} M. The adsorption and desorption behavior of chromate at the fused quartz/water interface was modeled using a model based on Langmuir adsorption and first-order chromate desorption. This model yielded an adsorption rate constant of $3(1) \times 10^3$ s^{-1} M^{-1} and a desorption rate constant of $9(7) \times 10^{-3}$ s^{-1}. These rate constants are in good agreement with desorption rate constants determined in individually measured chromate adsorption and desorption traces. At 300 K and pH 7, the resulting equilibrium constant for chromate binding is in good agreement with equilibrium constants obtained from Langmuir isotherm measurements carried out between pH 4 and 9. Thus, thermodynamic and kinetic measurements carried out in separate studies result in a standard free energy of chromate binding to fused quartz/water interfaces of 32 (+4/−3) kJ/mol and a corresponding chromate binding constant of 3.3×10^5 (($+17 \times 10^5$)/(-2.1×10^5)) M^{-1}. A simple model for chromate transport through geosorbents rich in silicate materials predicts that chromate will move <10% as far as groundwater, depending on sorbent porosity and density. Clearly, kinetic and thermodynamic data derived from more realistic interfaces other than the pristine fused quartz/water interface used in this work will provide more reliable estimates for predicting the migration potential of chromate in the environment, and this will be addressed in future studies.

Acknowledgment. K.A.G. acknowledges a Northwestern University Summer Research Fellowship for Undergraduates. We gratefully acknowledge equipment donations from Spectra Physics.

References and Notes

(1) Ellis, A. S.; Johnson, T. M.; Bullen, T. D. Chromium Isotopes and the Fate of Hexavalent Chromium in the Environment. *Science* **2002**, *295*, 2060−2062.

(2) Blowes, D. Tracking Environmental Chromium in Groundwater. *Science* **2002**, *295*, 2024−2025.

(3) Kavanaugh, M. C. *Alternatives for Groundwater Cleanup*; Academic Press: Washington, DC, 1994.

(4) Goyer, R. A.; Klaassen, C. D.; Waalkes, M. P. *Metal Toxicology*; Academic Press: New York, 1995.

(5) Katz, S. A.; Salem, H. *The Biological and Environmental Chemistry of Chromium*; VCH: New York, 1994.

(6) Nriagu, J. O.; Nieboer, E. *Chromium in the Natural and Human Environments*; John Wiley & Sons: New York, 1988.

(7) Pattison, D. I.; Davies, M. J.; Levina, A.; Dixon, N. E.; Lay, P. A. Chromium (VI) reduction by catechol(amine)s results in DNA cleavage in vitro: Relevance to chromium genotoxicity. *Chem. Res. Toxicol.* **2001**, *14*, 500−510.

(8) Holleman, A. F.; Wiberg, N. *Lehrbuch der Anorganischen Chemie*; W. de Gruyter: Berlin, New York, 1985.

(9) Chromium. In *National Research Council (US): committee on biologic effects of atmospheric pollutants*; National Academy of Sciences: Washington, DC, 1974; pp 125−145.

(10) Rubin, E. S. Toxic releases from power plants. *Environ. Sci. Technol.* **1999**, *33*, 3062−3067.

(11) Ribeiro, A. B.; Mateus, E. P.; Ottosen, L. M.; Bech-Nielsen, G. Electrodialytic removal of Cu, Cr, and As from chromate copper arsenate-treated timber waste. *Environ. Sci. Technol.* **2000**, *34*, 784−788.

(12) Helsen, L.; Van den Bulck, E. Metal behavior during the low-temperature pyrolysis of chromated copper-arsenate-treated wood waste. *Environ. Sci. Technol.* **2000**, *34*, 2931−2938.

(13) Baron, D.; Palmer, C. D.; Stanley, J. T. Identification of two iron-chromate precipitates in a Cr(VI)-contaminated soil. *Environ. Sci. Technol.* **1996**, *30*, 964−968.

(14) Greenwood, N. N.; Earnshaw, A. *Chemie der Elemente*; VCH Verlagsgesellschaft: Weinheim, 1990.

(15) Jardine, P. M.; Fendorf, S. E.; Mayes, M. A.; Larsen, I. L.; Brooks, S. C.; Bailey, W. B. Fate and transport of hexavalent chromium in undisturbed heterogeneous soil. *Environ. Sci. Technol.* **1999**, *33*, 2939−2944.

(16) August, E. E.; Mcknight, D. M.; HRNCIR, D. C.; Garhart, K. S. Seasonal variability of metals transport through a wetland impacted by mine drainage in the rocky mountains. *Environ. Sci. Technol.* **2002**, *36*, 3779−3786.

(17) Tokunaga, T. K.; Wan, J.; Firestone, M. K.; Hazen, T. C.; Schwartz, E.; Sutton, S. R.; Newville, M. Chromium diffusion and reduction in soil aggregates. *Environ. Sci. Technol.* **2001**, *35*, 3169−3174.

(18) Grossl, P. R.; Eick, M.; Sparks, D. L.; Goldberg, S.; Ainsworth, C. C. Arsenate and chromate retention mechanisms on Goethite. 2. Kinetic evaluation using a pressure-jump relaxation technique. *Environ. Sci. Technol.* **1997**, *31*, 32−326.

(19) Weng, C. H.; Huang, C. P.; Allen, H. E.; Leavens, P. B.; Sanders, P. F. Chemical interactions between Cr(VI) and hydrous concrete particles. *Environ. Sci. Technol.* **1996**, *30*, 371−376.

(20) Fendorf, S.; Eick, M. J.; Grossl, P.; Sparks, D. L. Arsenate and chromate retention mechanisms on Goethite. 1. Surface structure. *Environ. Sci. Technol.* **1997**, *31*, 315−320.

(21) Loyaux-Lawniczak, S.; Refait, P.; Ehrhardt, J.-J.; Lecomte, P.; Genin, J.-M. Trapping of Cr by formation of ferrihydrate during the reduction of chromate ions by Fe(II)-Fe(III) hydroxysalt green rust. *Environ. Sci. Technol.* **2000**, *34*, 438−443.

(22) Buerge, I. J.; Hug, S. J. Influence of mineral surfaces on chromium(VI) reduction by iron(II). *Environ. Sci. Technol.* **1999**, *33*, 4285−4291.

(23) Langmuir, D. *Aqueous Environmental Geochemistry*; Prentice-Hall: Upper Saddle River, NJ, 1997.

(24) Deng, B.; Stone, A. T. Surface-catalyzed chromium (VI) reduction: reactivity comparisons of different organic reductants and different oxide surfaces. *Environ. Sci. Technol.* **1996**, *30*, 2484−2494.

(25) Deng, B.; Stone, A. T. Surface-catalyzed Chromium(VI) reduction: The TiO2−Cr(VI)-Mandelic Acid System. *Environ. Sci. Technol.* **1996**, *30*, 463−472.

(26) Buonicore, A. J. *Cleanup Criteria for Contaminated Soil and Groundwater*; ASTM: West Conshohocken, PA, 1996.

(27) Mifflin, A. L.; Gerth, K. A.; Weiss, B. M.; Geiger, F. M. Surface Studies of Chromate Binding to Fused Quartz/Water Interfaces. *J. Phys. Chem. A* **2003**, *107*, 6212−6217.

(28) Hicks, J. M.; Urbach, L. E.; Plummer, E. W.; Dai, H. L. Can Pulsed Radiation of Surfaces be Described by a Thermal Model? *Phys. Rev. Lett.* **1988**, *61*, 2588.

(29) Sandrock, M. L.; Pibel, C. D.; Geiger, F. M.; Foss, C. A. Synthesis and second-harmonic generation studies of noncentrosymmetric gold nanostructures. *J. Phys. Chem. B* **1999**, *103*, 2668−2673.

(30) Shen, Y. R. *The Principles of Nonlinear Optics*; John Wiley & Sons: New York, 1984.

(31) Shen, Y. R. Surface properties probed by second-harmonic and sum-frequency generation. *Nature* **1989**, *337*, 519−525.

(32) Eisenthal, K. B. Liquid interfaces probed by second-harmonic and sum-frequency spectroscopy. *Chem. Rev.* **1996**, *96*, 1343−1360.

(33) Shen, Y. R. Surfaces probed by nonlinear optics. *Surf. Sci.* **1994**, *299/300*, 551−562.

(34) Eisenthal, K. B. Equilibrium and dynamic processes at interfaces by second harmonic and sum frequency generation. In *Annual Review of Physical Chemistry*; Strauss, H. L., Babcock, G. T., Leone, S. R., Eds.; Annual Reviews Inc.: Palo Alto, CA, 1992; Vol. 43, pp 627−661.

(35) Heinz, T. F. *Nonlinear Surface Electromagnetic Phenomena*; Elsevier Publishers: 1991.

(36) Jung, L. S.; Campbell, C. T. Sticking probabilities in adsorption from liquid solutions: Alkylthiols on gold. *Phys. Rev. Lett.* **2000**, *84*, 5164−5167.

(37) Jung, L. S.; Campbell, C. T. Sticking probabilities in adsorption of alkanethiols from liquid ethanol solution onto gold. *J. Phys. Chem. B* **2000**, *104*, 11168−11178.

(38) Georgiadis, R.; Peterlinz, K. P.; Peterson, A. W. Quantitative measurements and modeling of kinetics in nucleic acid monolayer films using SPR spectroscopy. *J. Am. Chem. Soc.* **2000**, *122*, 3166−3173.

(39) Bond, W. N.; Puls, H. O. *Philos. Mag.* **1937**, *7*, 864−888.

(40) Iadicicco, N.; Paduano, L.; Vitagliano, V. Diffusion Coefficients for the System Potassium Chromate−Water at 25 °C. *J. Chem. Eng. Data* **1996**, *41*, 529−533.

(41) Adamson, A. W. *Physical Chemistry of Surfaces*, 5th ed.; John Wiley & Sons: New York, 1990.

(42) Karpovich, D. S.; Blanchard, G. J. Direct Measurement of the Adsorption Kinetics of Alkanethilate Self-Assembled Monolayers on a Microcrystalline Gold Surface. *Langmuir* **1994**, *10*, 3315−3322.

(43) Levich, V. G. *Physicochemical Hydrodynamics*; Prentice Hall: Englewood Cliffs, NJ, 1962.

(44) Atkins, P. W. *Physical Chemistry*, 6th ed.; Oxford University Press: 1998.

(45) Fogler, H. S. *Elements of Chemical Reaction Engineering*, 3rd ed.; Prentice Hall PTR: Upper-Saddle River, NJ, 1999.

(46) Froessling, N. *Gerlands Beitr. Geophys.* **1938**, *52*, 170.

(47) Laidler, K. J.; Meiser, J. H. *Physical Chemistry*; The Benjamin Cummings Publishing Company: Menlo Park, CA, 1982.

(48) U.S. Environmental Protection Agency. Understanding Variation in Partition Coefficient, Kd, Values: Introduction. Report available on the web at www.epa.gov/radiation/cleanup/partition.htm, 2002.

(49) Rai, D.; Zachara, J. M.; Eary, L. E.; Ainsworth, C. C.; Amonette, J. E.; Cowan, C. E.; Szelmeczka, R. W.; Resch, C. T.; Schmidt, R. L.; Girvin, D. C.; Smith, S. C. *Chromium Reactions in Geoloical Materials*; Electric Power Research Institute: 1988.